Stability analysis and long-term behaviour of deep tunnels in clay formations

Arnaud Dizier[1]*, Marc Scibetta[2], Gilles Armand[3], Jad Zghondi[3], Temenuga Georgieva[1], Guangjing Chen[1], Jan Verstricht[1], Xiangling Li[1], Didier Léonard[4] and Severine Levasseur[4]

[1]European Underground Research Infrastructure for Disposal of Nuclear Waste in Clay Environment (EURIDICE), Boeretang 200, 2400 Mol, Belgium

[2]SCK CEN, Belgian Nuclear Research Centre, Institute for Nuclear Materials Science, Boeretang 200, 2400 Mol, Belgium

[3]ANDRA, French National Radioactive Waste Management Agency, RD 960, BP9, 55290 Bure, France

[4]ONDRAF/NIRAS, Avenue des arts 14, B-1210 Bruxelles, Belgium

AD, 0000-0002-7353-2222

*Correspondence: arnaud.dizier@euridice.be

Abstract: Demonstrating the feasibility of constructing tunnels in deep clay formations is an important goal of the Belgian RD&D programme on the geological disposal of radioactive waste. In 2002 a major achievement was reached when the HADES Underground Research Laboratory (URL) in Boom Clay was extended with the construction of the Connecting Gallery. This demonstrated that it is feasible to construct galleries in poorly indurated clays using industrial techniques. To monitor the mechanical behaviour of the gallery and assess its stability, strain gauges were embedded in the segmental gallery lining and prisms were installed on the segments. These sensors provide valuable information that will support the design of future galleries. This paper presents 20 years of monitoring data in the Connecting Gallery and a first analysis of these data in terms of Boom Clay behaviour. In addition, the key findings are compared with those of a similar analysis performed by Andra (the French Radioactive Waste Agency) at the Meuse/Haute-Marne URL. The latter URL is excavated in the Callovo-Oxfordian claystone. The comparison identifies general trends and highlights similarities between the behaviour of tunnels in poorly indurated clay (Boom Clay) and in claystone.

RD&D (research development & demonstration) in the field of the long-term management of high-level and/or long-lived radioactive waste was initiated in 1974 in Belgium by the Belgian Nuclear Research Centre (SCK CEN). A decade later, the responsibility for the RD&D programme was transferred to ONDRAF/NIRAS (ONDRAF/NIRAS 2013). Since the early 1980s, the programme has benefitted from a dedicated underground research laboratory (URL), the HADES (High-Activity Disposal Experimental Site) URL in Mol (Fig. 1, Li *et al.* 2023). The URL, which is currently managed by EIG EURIDICE, allows *in situ* characterization of the Boom Clay to be performed and technologies to construct, operate and close a deep geological repository to be tested, demonstrated and optimized.

The Boom Clay is characterized as a poorly indurated clay with a visco-elasto-plastic behaviour. The clay has an isotropic elastic modulus of 300 MPa and a Poisson's ratio of 0.125. The drained cohesion is 300 kPa and the friction angle is 18° (Bernier *et al.* 2007). This set of parameters constitutes the basic parameters of the clay and more advanced parameters are detailed in Chen *et al.* (2023) and in Villar *et al.* (2020).

The excavation and supporting/lining techniques used for the HADES URL have evolved over the lifetime of the URL. It all started with the construction of the first shaft and the first gallery, at a depth of 225 m below the surface in Boom Clay. At that time, the Boom Clay mechanical behaviour at this depth was poorly understood. It was thought that the Boom Clay would not be able to sustain the excavation work (de Beer *et al.* 1977; Bastiaens *et al.* 2006). Therefore, the Boom Clay was frozen prior to the excavation works. The excavation itself was done using conventional mechanical methods (pneumatic drilling) and the ground support was made from cast iron segments.

This construction technique was, however, expensive and is economically not viable for constructing a full-scale deep geological repository. Therefore, a series of experiments were conducted to demonstrate the feasibility of excavating in

From: Li, X. L., Van Geet, M., Bruggeman, C. and De Craen, M. (eds) 2023. *Geological Disposal of Radioactive Waste in Deep Clay Formations: 40 Years of RD&D in the Belgian URL HADES.*
Geological Society, London, Special Publications, **536**, 185–204.
First published online May 22, 2023, https://doi.org/10.1144/SP536-2022-86

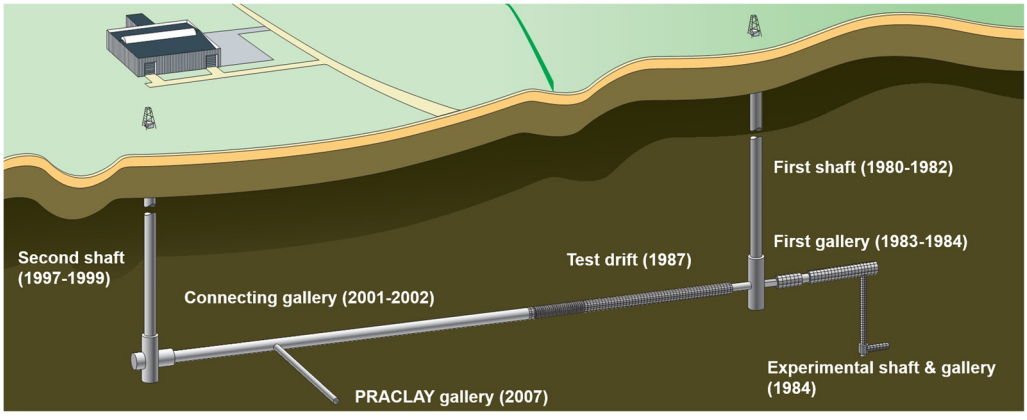

Fig. 1. Layout of the underground research laboratory at Mol, Belgium. Source: ©EIG EURIDICE.

unfrozen clay at this depth. In addition, a lighter ground support was tested with the construction of the experimental shaft and gallery in 1984 and was then used for the construction of the Test Drift in 1987. The Test Drift is supported by 60 cm thick concrete segments, separated by wooden plates to allow for some deformation of the structure and thus limiting the stresses within the support.

A flexible ground support made from sliding steel ribs was also tested in an extension of the Test Drift, called the Andra gallery. This specific lining was constructed with the support of Andra as part of their programme on the mechanical behaviour of deep clay formations and was co-financed by the EU (Rousset 1988, 1990). It is this type of lining that is being used in Andra's URL in Bure.

The period when the first URL, the Test Drift and the Andra gallery were constructed, is called the 'pioneering phase'. The techniques used during this phase were semi-manual (Fig. 2) and an excavation rate of only 2 m per week was achieved (Funcken *et al.* 1983; Neerdael *et al.* 1992; Bernier *et al.* 2007).

The next phase in the construction history of the HADES URL was the 'industrial phase'. It consisted of the construction of the second shaft and the gallery (called 'Connecting Gallery') connecting the second shaft to the URL part constructed during the

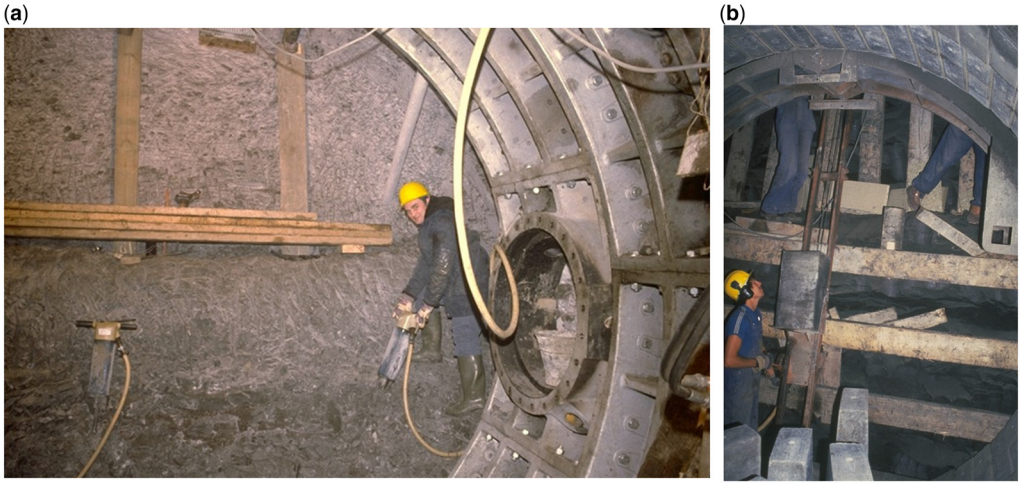

Fig. 2. (**a**) Construction of the first gallery lined with cast-iron segments. (**b**) Photograph taken during the construction of the Test Drift with semi-manual techniques. Each ring is composed of 64 concrete blocks (60 cm thick) with wooden plates between the segments. Source: ©EIG EURIDICE.

pioneering phase. The shaft and Connecting Gallery were constructed using industrial techniques. The Connecting Gallery was excavated using a road header tunnel boring machine (TBM) without front support. Using this excavation technique, a progress rate of between 2 and 4 m per day could be achieved.

In 2007, a 45 m long gallery called the PRACLAY Gallery was built perpendicular to the Connecting Gallery. This demonstrated the feasibility of constructing smaller-diameter galleries and T-crossings in Boom Clay using industrial techniques similar to those used for the Connecting Gallery. The PRACLAY Gallery was then equipped with a heating system and dedicated instrumentation for the follow-up of the PRACLAY Heater Test (Van Marcke *et al.* 2013). This test started in 2014 and heats the clay to 80°C for 10 years at the interface between the concrete lining and the Boom Clay (Dizier *et al.* 2016, 2021).

Owing to their favourable properties for containing radioactive waste, France also considers clays as a potential host rock for geological disposal. At the beginning of the 2000s, Andra (the French National Radioactive Waste Management Agency) began the construction of the Meuse/Haute-Marne URL in the Callovo-Oxfordian formation. A large experimental programme in science and technology (Delay *et al.* 2007) has been implemented in this URL. One of the main goals of this programme is the development of construction methods and the optimization of repository structures (Armand *et al.* 2015).

Since 2006, an important programme was launched to study the impact of different excavation and support techniques and to test possible tunnelling techniques for the Cigéo project (the French high-level and intermediate-level long-lived radioactive waste deep geological repository). Parallel galleries are built far enough apart with different construction methods and support structures (Zghondi *et al.* 2015). One of these galleries was built with comparable techniques to those used for the construction of the Connecting Gallery of the HADES URL, the GRD4 gallery: a 89 m long gallery drilled along the major horizontal stress direction of the URL using a tunnel boring machine with a road header. The gallery is supported by a segmental lining consisting of reinforced concrete segments and backfilled with two types of grout: a conventional grout and a compressible one (Carraretto *et al.* 2015). The objective of the construction of this gallery is not to achieve 'industrial' rates but to analyse the response of the Callovo-Oxfordian claystone during the excavation, especially the interaction between the clay and the segments, and to follow the long-term stress evolution in the segments.

Understanding the short- and long-term behaviour of galleries is critical to optimize the support design of a future deep geological repository as the galleries need to remain open and stable for decades. This article presents the deformations measured within the Connecting Gallery of the HADES URL and compares these with deformations measured within the GRD4 gallery of the Meuse/Haute-Marne URL. The evolution of these observed deformations and their interpretation in term of stresses in the lining provide insight into the short- and long-term behaviour of galleries in Boom Clay and Callovo-Oxfordian claystone. This shared understanding will be beneficial for the feasibility studies on deep geological repositories in clay and claystone formations.

Construction and instrumentation of the galleries in the HADES and Meuse/Haute-Marne URLs

The Connecting Gallery at the HADES URL

Gallery construction. The Connecting Gallery was constructed within 6 weeks in February and March 2002 using industrial techniques. An open shield tunnel boring machine equipped with a road header was used to excavate the clay. The tunnelling shield was equipped with adjustable cutting edges to adjust the over-excavation diameter and to steer the TBM (Bastiaens *et al.* 2003).

The gallery has a total length of more than 85 m and its lining consists of concrete segmental lining (wedge-blocks technique) (Fig. 3). The lining is composed of 83 rings of unreinforced C75/90 concrete using CEM II/B-V42.5 cement. Each ring is 1 m long, 40 cm thick and consists of 10 segments and two keys.

The progress rate was about 2–4 m per day, which is 10 times higher than what was achieved during the construction of the older part of the URL. This demonstrated that by using industrial techniques it is technically and economically feasible to construct tunnels in poorly indurated clay.

Instrumentation of the gallery. To monitor the mechanical evolution of the segmental lining, vibrating wire strain gauges with a measuring base of 150 mm were embedded in concrete segments. These were placed 10 cm from the intrados and from the extrados of rings 15, 30 and 50 (Fig. 4). Two configurations were implemented: a 6-gauge segment and a 12-gauge segment (Fig. 5; Bastiaens *et al.* 2003; Bernier *et al.* 2003; Verstricht *et al.* 2022).

The installation of the strain gauges was done by fixing them to a metal frame. This frame was then positioned in the mould using plastic distance holders and concrete was poured into the mould. An

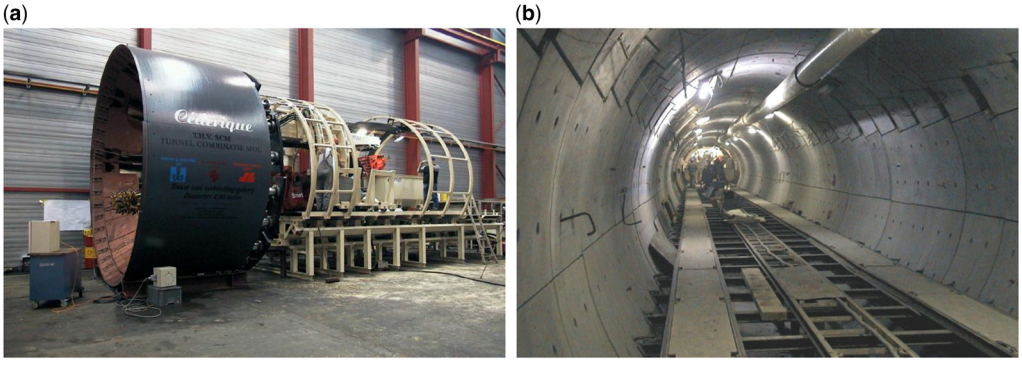

Fig. 3. (**a**) Tunnel boring machine equipped with a shield and a road header. (**b**) Connecting Gallery during its construction. Each ring is composed of 10 segments (40 cm thick) and two counter key segments (Bastiaens *et al.* 2003).

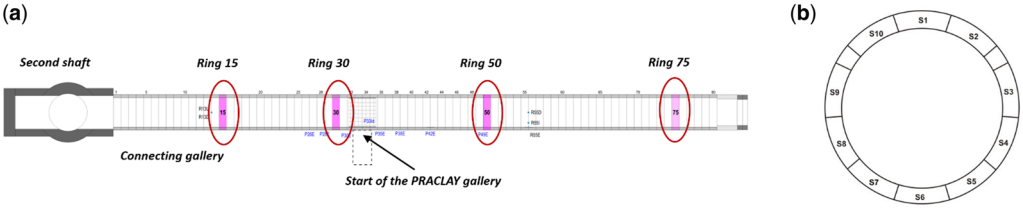

Fig. 4. (**a**) Position of the three instrumented rings in the Connecting Gallery. (**b**) Numbering of the segments in one ring (6-gauge segments: S2, S3, S5, S7, S9 and S10; 12-gauge segments: S1, S4, S6, S8). Source: modified from Verstricht *et al.* (2022), ©2022, with permission from Elsevier.

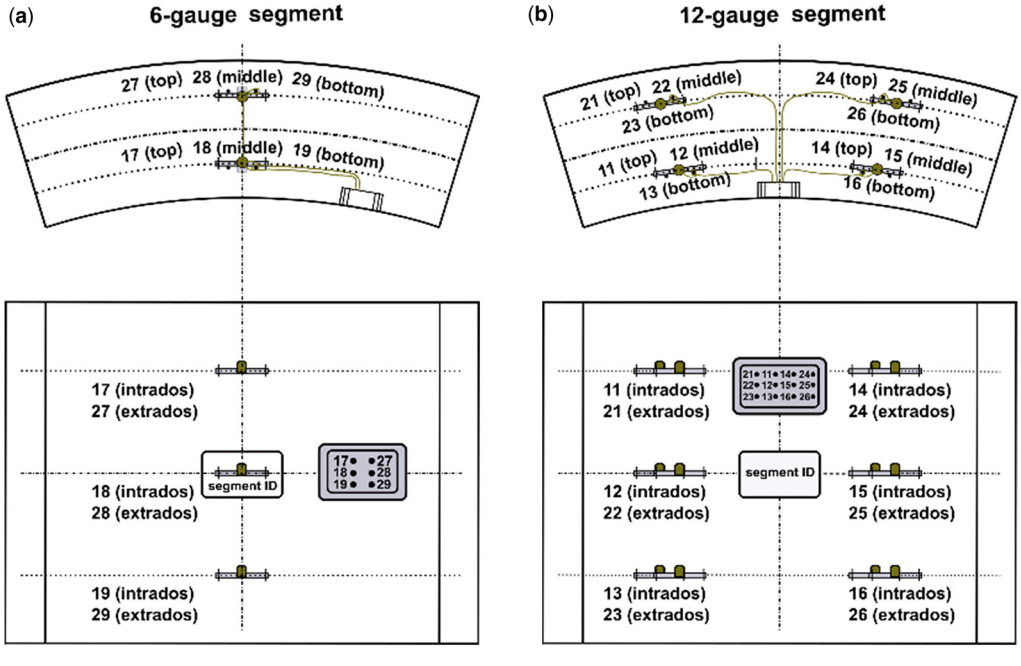

Fig. 5. Layout of the instrumentation for the embedded strain gauges with three (**a**) or six (**b**) strain gauges close to the intrados and the extrados. Source: after Bernier *et al.* (2003).

example of one instrumented cage with a 12-gauge configuration can be seen in Figure 6.

A total of 270 vibrating wire strain gauges were installed in the concrete segments to measure the circumferential strain. Only two have shown deviating measurements, indicating that these sensors are defective (Verstricht *et al.* 2022). This good result raises the expectation that the sensors will allow continued monitoring of the gallery for a longer period of time. This will be beneficial for assessing the stability and understanding the long-term soil–structure interaction between the clay and the lining.

The GRD4 gallery at the Meuse/Haute-Marne URL

Gallery construction. Similar construction techniques to that one used for the Connecting Gallery in HADES URL were tested at the Meuse/Haute-Marne URL in Bure. In particular, the GRD4 gallery was excavated in 2013 using a TBM specifically manufactured by Herrenknecht. This TBM includes a road header under a shield with a diameter of 6.27 m (Fig. 7). The gallery is 89 m long and has an inner diameter of 5.10 m. The gallery is lined with a segmental concrete lining (Fig. 8) that is 80 cm thick and consists of 93 rings, plus six 'false rings'. The reinforced segments were prefabricated using a C60/75 class of concrete. Contrary to the Connecting Gallery built in Boom Clay, the annual gap between the GRD4 gallery and the Callovo-Oxfordian claystone is grouted with mortar (Carraretto *et al.* 2015; Zghondi *et al.* 2015).

The gallery lining can be divided into three zones. The first zone is 36 m long and is grouted with a conventional mortar type. The next zone consists of an 8 m long transition zone and a 30–40 m long zone where a compressible grout is used. Finally, a 10 m long zone is used for the TBM disassembly. The grouting was injected through a socket embedded in the segments (70 mm diameter). On each pumping intervention, segments were grouted on three different levels (Fig. 7a) to respect the identified mortar slope (25° for the compressible mortar and 30° for the conventional mortar). The final injection of the vaulted segment is reached just under 20 m from the working face.

The excavation works were performed using three teams that worked 5 days per week. They progressed at an average rate of 4.67 rings per week (0.79 m per day). The excavation was completed within 6 months between June and November 2013.

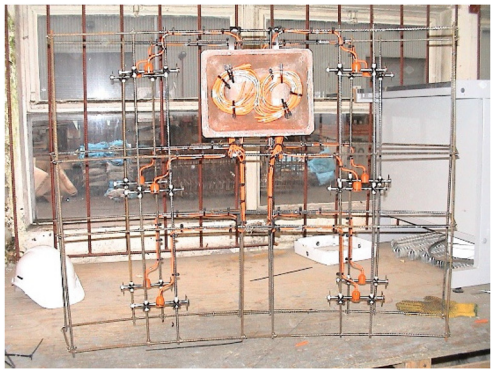

Fig. 6. Framework used to maintain the strain gauges at their position during the concrete pouring, a 12-gauge configuration (Bastiaens *et al.* 2003).

Instrumentation of the gallery. To monitor the mechanical behaviour of the structure, in particular strains and stresses in the concrete lining, as well as the compression of the grout mortar, four rings (eight segments/ring – the key segment is not instrumented) were equipped in Stradal's manufactory. Three total pressure cells and eight strain gauges were installed on the reinforcement of each segment

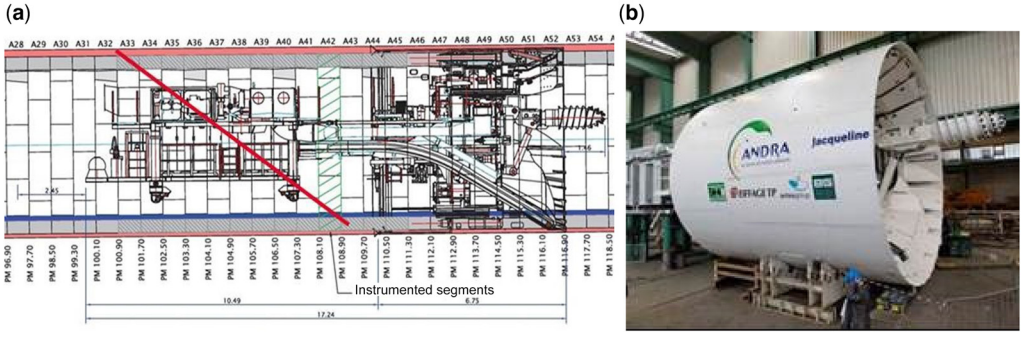

Fig. 7. Views of the tunnel boring machine (Carraretto *et al.* 2015; Zghondi *et al.* 2015).

Fig. 8. View of the GRD4 gallery with the segmental concrete lining (Armand *et al.* 2015).

of the four monitored rings. An instrumented segment was deposited on the GRD4 gallery (not installed on any ring) to serve as reference segment (not mechanically loaded).

The instrumentation of the segments was based on feedback from other experiments (such as those carried out at the HADES URL for the Connecting Gallery). Vibrating wire strain gauges are used to measure orthoradial deformations. Total pressure cells were also installed in the structure. The instrumentation was installed by connecting it to the steel reinforcement of the segments prior to the pouring of the concrete (Fig. 9). As soon as the segments left the production line, the deformations in the concrete could be monitored to measure the behaviour of the segments during all phases of its lifetime. In a ring, all segments are instrumented except the key segment (V9 in Fig. 9b), which is too strongly reinforced.

Monitoring results in the Connecting Gallery

Since 2002, the strain gauges have been monitored manually on a regular basis. This section presents the monitoring results obtained with the vibrating wire strain gauges embedded in the segments of three instrumented concrete rings. The measurements from these strain gauges are very similar. Therefore, the results for two segments will be discussed first before looking at the measurements of all rings.

An example of the evolution of the strain as a function of time can be seen in Figures 10 and 11. These figures show the results for two segments of ring 30 near the PRACLAY Gallery (which intersects the Connecting Gallery at rings 33–34). These segments illustrate the main phenomena observed in all of the instrumented segments. The convention of sign adopted in this paper is the one from soil–rock mechanics whereby compressive strains and stresses are positive. The evolution of the strain can be observed in the segment S2 (a six-strain gauge configuration) and in segment S6 (a 12-strain gauge configuration). For these two figures, all strain gauge measurements present a similar pattern which can be summarized as follows:

- an initial significant increase of the strain when the ring is installed;
- the strain continues to increase over time, but at a slower rate;
- the strains at intrados and extrados follow the same pattern as described above but with a different magnitude;
- at the bottom of the ring (segment S6), while the extrados continues to deform with time, the deformation at the intrados seems to stabilize.

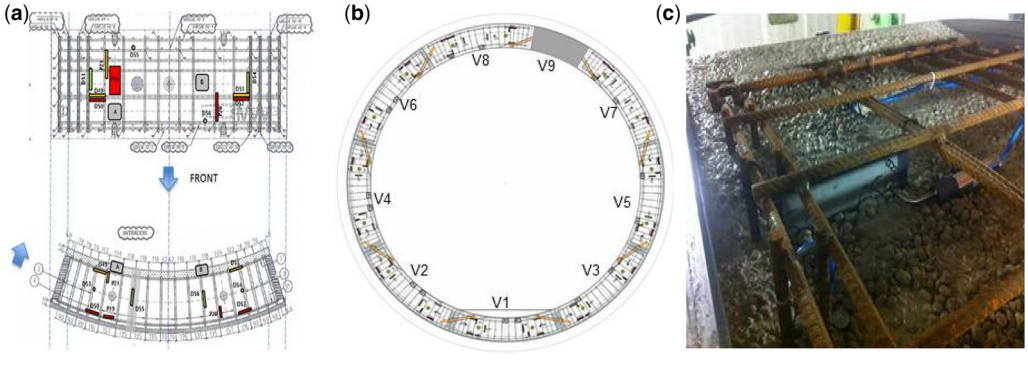

Fig. 9. (**a**) Scheme of the location of vibrating strain gauge wire and total pressure sensors in a segment and (**b**) in a ring (64 strain gauges and 24 total pressure sensors). (**c**) Photograph of the concrete pouring into the mould with the reinforcement bar and the total cells.

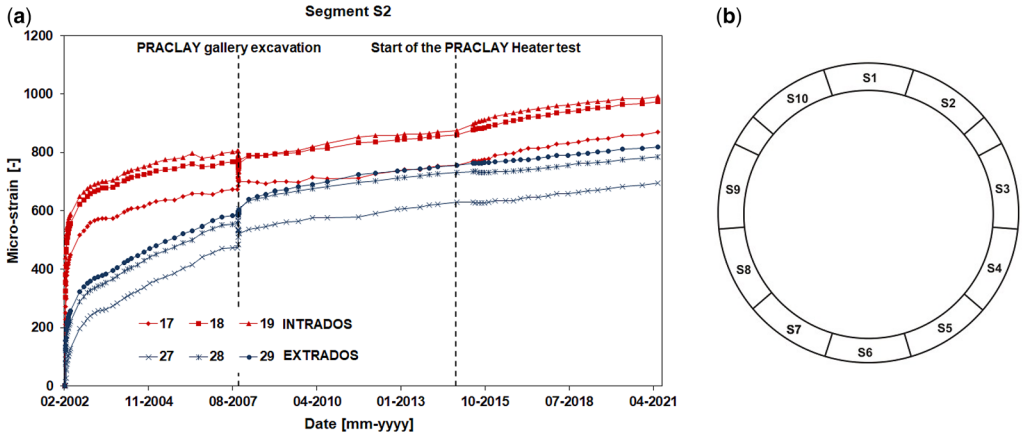

Fig. 10. Evolution of the strain monitored in the S2 segment of ring 30 (6-gauge configuration segment: three at the intrados (17, 18 and 19) and three at the extrados (27, 28 and 29)).

The position of ring 30 close to the PRACLAY Gallery allows observation of how the strain changes owing to the excavation of the PRACLAY Gallery in 2007 (Figs 10 & 11). In November 2014, the PRACLAY Heater Test started (Dizier *et al.* 2021). The monitoring frequency was increased and it was observed that the heating of the PRACLAY Gallery induced a modification of the stress field around the Connecting Gallery as the strains evolved at a different rate. This is a mechanical effect caused by the heating and pressurization of the PRACLAY Gallery.

Figures 12 and 13 show the evolution of the averaged strain, ring by ring, at the intrados and at the extrados, respectively. These figures make it clear that the strains evolve differently between the intrados and the extrados and that the strain evolution depends on the angular position in the ring. At the crown (top of the ring) and invert (lowest point of the ring) of the tunnel, the strain at the intrados seems to stabilize after having reached 'a limit', while at the extrados the strain keeps increasing. At the springline (horizontal line crossing the tunnel axis), the opposite is observed. A kind of plateau (slightly increasing or decreasing) is reached for the extrados while at the intrados the strain continuously increases. This comparable evolution between the three instrumented rings validates the setup and the results.

The evolution of strain is smooth without any sharp or sudden variations except for ring 30 that exhibited a small and sudden variation after 2000 days, induced by the excavation of the PRACLAY gallery in its vicinity, but this disturbance is very limited in time. This indicates that the tunnel lining is stable during this monitoring period. This provides useful information for the future safety and operation of the URL.

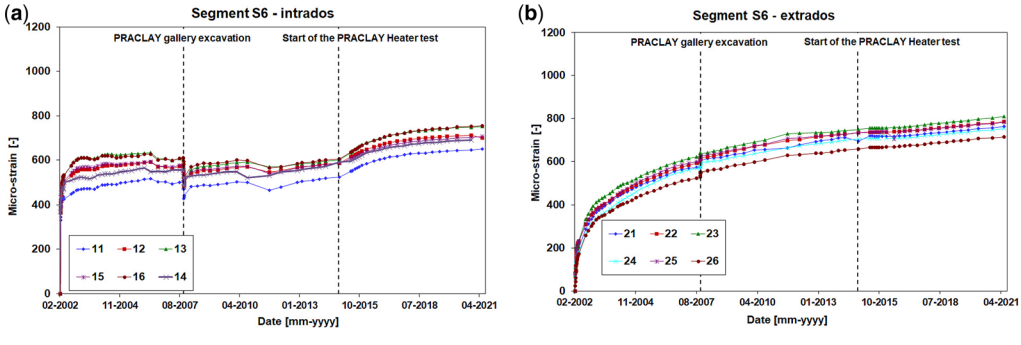

Fig. 11. Evolution of the strain monitored in the S6 segment of ring 30, which is a 12-gauge segment (six intrados and six extrados): (**a**) six strain gauges close to the intrados and (**b**) six strain gauges close to the extrados.

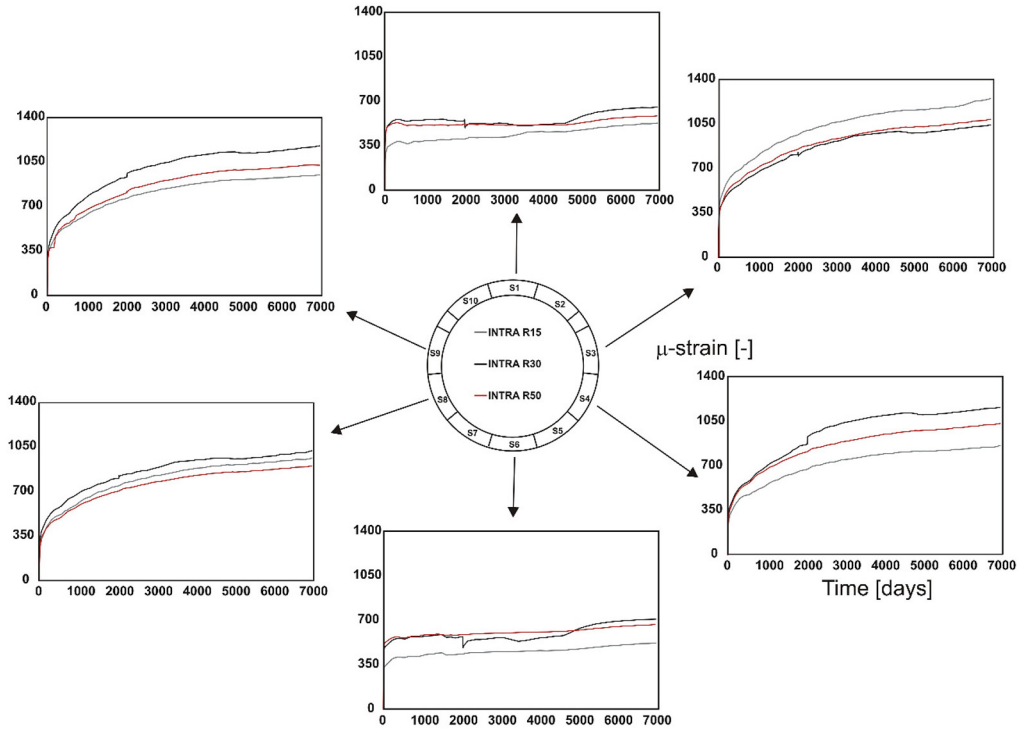

Fig. 12. Strain measured (μ-strain) as a function of time (days) at the intrados of the lining of rings 15, 30 and 50.

Figure 14 presents the distribution of the strain along the angular position at different times. In 2002 and 2004, the distribution at intrados and at extrados along the circumference is rather uniform. With time, however, the gallery shows an oval distortion and the strain distribution is no longer uniform. The deformation at intrados at 90° and at 270° (at the springline) increases while it almost stabilizes at 0° and at 180° (at the crown and at the invert). At the extrados the opposite happens with an increase at the crown and at the invert (0° and 180°) and almost stabilization at 90° and 270° along the springline.

The evolution of the strain can be divided into two phases. In the short-term period, the pressures applied on the lining of the excavated gallery are nearly isotropic and the related strain distribution remains fairly uniform. In the longer term, the applied pressures gradually tend to restore the *in situ* stress conditions before the excavation. They are anisotropic and defined by the coefficient of earth pressure at rest K_0 (ratio of effective stresses by definition), which is about 0.7 at the level of the HADES URL. As a result, the deformation mode is amplified with an increase in distortion of the lining and an increase in the difference between the strains in the horizontal and in the vertical direction.

In addition to the strain gauges, prisms were attached at the surface of the concrete segments of nine rings (R8, R18, R26, R41, R42, R50, R59, R69 and R81). A topographical survey can be conducted to monitor the convergence of the lining. The convergence measurements are, however, affected by noise. In order to give a clearer picture of the lining convergence, an ellipse was fitted on the measurements made at each time step. The semi-major axis (a in Fig. 15) and the semi-minor axis (b in Fig. 15) of this ellipse indicate how the lining convergence evolves over time. Figure 15 presents the results of this fitting. Nearly 20 years after the start of the monitoring survey in 2004, the semi-minor axis decreased by almost 4 mm and the semi-major increased by almost 8 mm.

These long-term observations allow the conclusion to be drawn that the tunnel deforms into a lying-egg shape: its horizontal diameter increases while its vertical diameter decreases. Figure 16 shows the deformation mode of the lining. At the intrados, a high compression is observed at the level of the springline while the compression is rather limited at the crown and invert of the lining.

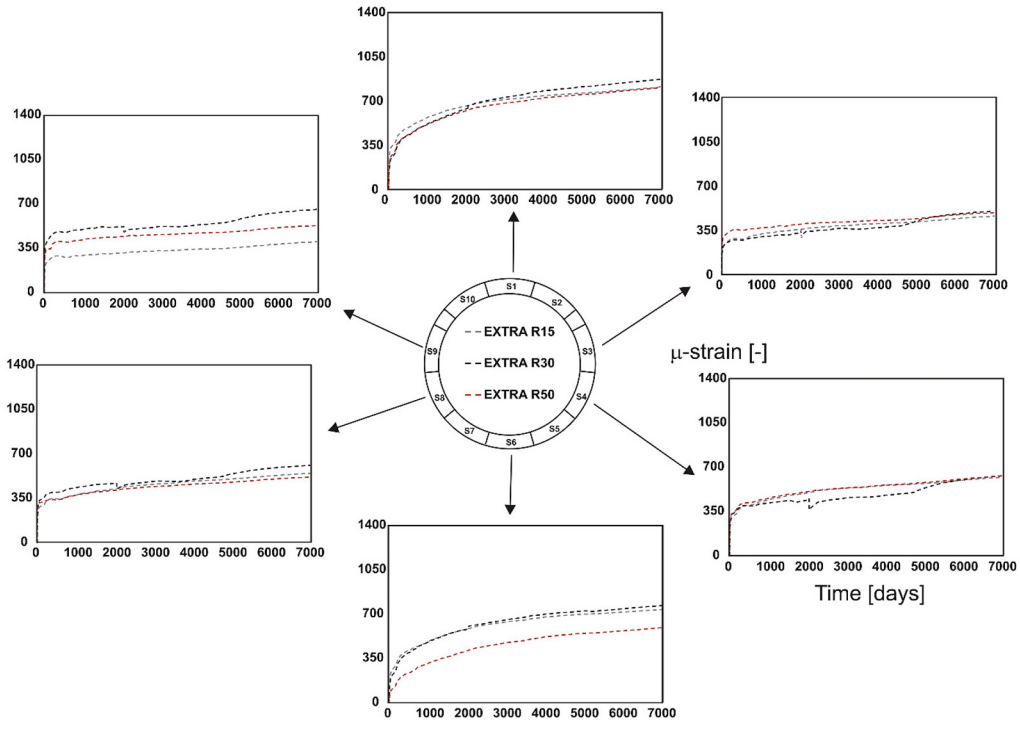

Fig. 13. Strain measured (μ-strain) as a function of time (days) at the extrados of the lining of rings 15, 30 and 50.

At the extrados, the opposite is observed. The compression at the springline location is limited while the compressive strain in the vertical direction (crown and invert) continuously increases.

This behaviour is different from what is observed in the very short term. Shortly after the excavation of the gallery in 2002, the distributions were rather uniform along the angular position (Fig. 14). A closer look at the distribution of strains during the first months after excavation (see the distribution of strains at intrados and extrados in Fig. 17) shows that the compressive strains at the intrados are slightly higher at the crown and at the invert compared with the springline. The reverse is true for the strains at the extrados. This very short-term deformation mode is the opposite of the long-term deformation mode described earlier: the ovalization is in the vertical direction and not in the horizontal

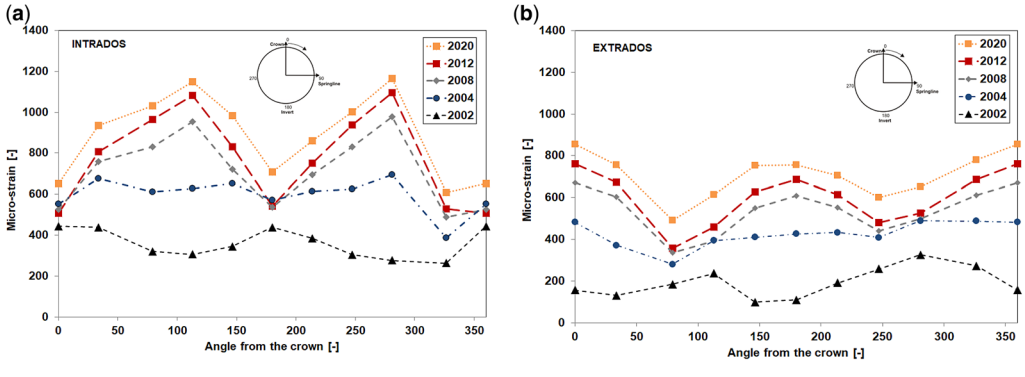

Fig. 14. Distribution of the strain (averaged over the segment) along the angular position of the tunnel in ring 30 at the location of the sensors at (**a**) the intrados and (**b**) the extrados.

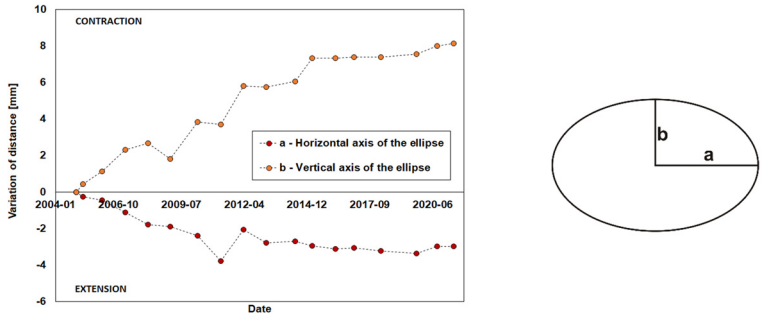

Fig. 15. Evolution of the semi-major axis and the semi-minor axis of an ellipse fitted based on the topographical original data since the beginning of the survey.

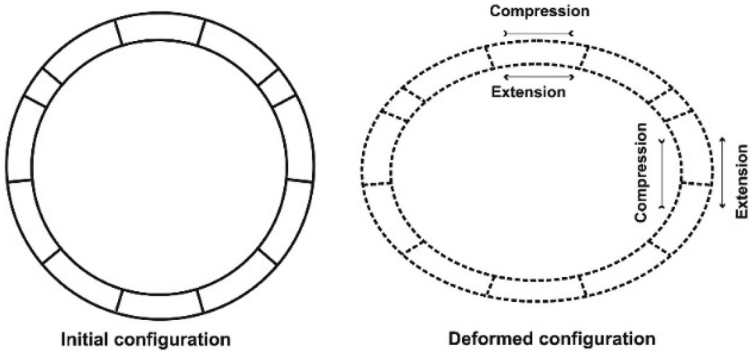

Fig. 16. Observed deformation of the lining in a lying-egg shape.

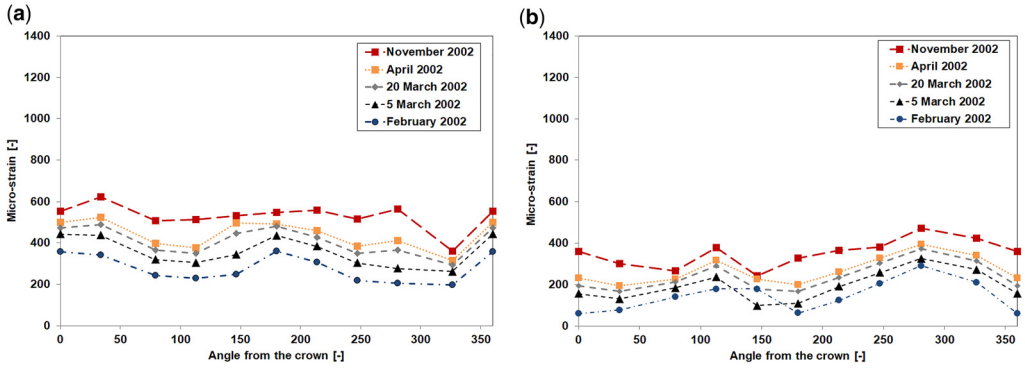

Fig. 17. Distribution of the strain (averaged over the segment at the intrados and the extrados) along the circumference of the tunnel in ring 30 at (**a**) the intrados and (**b**) the extrados focusing on the short-term evolution.

one. This was also observed during the excavation work of the Connecting Gallery where, according to Bastiaens *et al.* (2003), the contact between the tunnel walls and the shield first appeared in the horizontal direction.

This distinct behaviour between the short and long term can be explained by the anisotropic properties of the clay and the formation of an excavation damaged zone around galleries, as demonstrated by hollow cylinder tests that simulate in

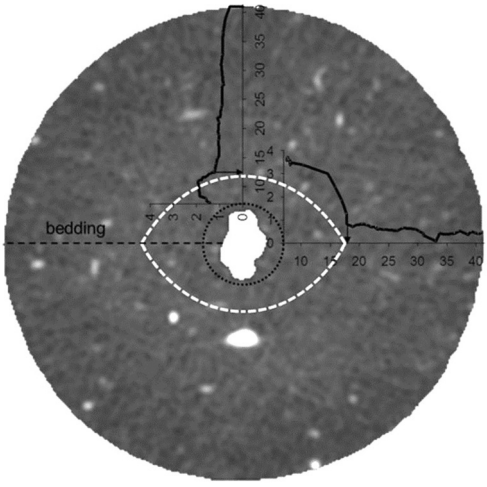

Fig. 18. Eye-shaped damage zone (white dashed line) around the central hole (black dotted line) of a hollow cylinder test in Boom Clay. The black curves correspond to the measured displacements, with their corresponding axis, around the central hole (Labiouse *et al.* 2014), and the black dashed line indicates the orientation of the bedding.

the laboratory the gallery excavation (Labiouse *et al.* 2014). In such tests, gallery excavation is simulated by the decreasing pressure in the central hole. Owing to this unloading, the ovalization of the hole occurs with a higher convergence in the horizontal direction (parallel to bedding) than in the vertical one (perpendicular to bedding) (Fig. 18). This induces an eye-shaped damage zone (white dashed curves in Fig. 18) around the hole, corresponding to the chevron-like fracture pattern observed during the construction of the Connecting Gallery (Fig. 19) and described by Mertens *et al.* (2004). François *et al.* (2014) have shown that the eye-shaped damaged zone simulated by hollow cylinder tests can be modelled by considering anisotropic properties of the Boom Clay combined with a variation of the effective cohesion as a function of the angle to the bedding in the Drucker–Prager criterion. This modelling approach reproduces, for this laboratory test, the development of shear bands in the excavation damaged zone and the associated anisotropic convergences. In *in situ* conditions, the direct contact between the clay and the lining and the subsequent recompression of the clay on the lining with time significantly limit the development of these shear bands (Salehnia 2015). The model proposed by François *et al.* (2014) is insufficient to reproduce the observed mechanical effects and its deformation mode developing after the excavation of a gallery. To go further, such a model should be extended by considering the visco-plastic behaviour of the clay, causing the load on the lining to increase with time. To conclude, the anisotropic properties of the Boom Clay affect the gallery lining–clay behaviour in the short term. In the long term, however, the soil–structure interaction is mainly controlled by the anisotropic *in situ* state of stress, which deformed the lining into a lying-egg shape that evolves with time.

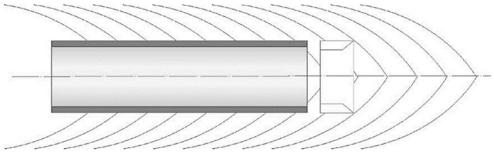

Fig. 19. Schematic representation of the encountered shear planes during the construction of the Connecting Gallery. Source: reprinted from Mertens *et al.* (2004), ©2004, with permission from Elsevier.

Stress analysis in the segmental concrete lining of the Connecting Gallery

The stresses in the lining are the result of the interaction between the gallery and clay deformation. By measuring these stresses, important information can be derived about the clay state and the evolution of the pressure acting on the gallery. Knowledge of the stresses in the concrete segment also allows to evaluate the methodology used to design the gallery and to obtain safety factors against rupture of the segments.

Based on the measured strains, the stresses in the lining segments were calculated considering the time-dependent behaviour of the concrete as defined in Eurocode2 (EN 1992-1-1 2004). This model decomposes the total strain into an elastic and a time-dependent one. The time-dependent strain includes the creep and shrinkage strains of the concrete.

The time-dependent Eurocode2 model was developed on the basis of the CEB-FIP Model (1990). This empirical model represents the visco-elastic behaviour of the concrete by introducing the creep of the concrete as a function of a series of factors which depend on the variations of environmental conditions (e.g. humidity or temperature). In this article, only a summary of the main equations is proposed. A complete description of the model is given in Eurocode2 (EN 1992-1-1 2004).

The creep coefficient $\phi_{cr28}(t, t_0)$ is calculated for some arbitrary time t and an age of the concrete t_0 at first loading with:

$$\phi_{cr28}(t, t_0) = \phi_{c0} \cdot \beta(t, t_0) \quad (1)$$

where ϕ_{c0} is a notional creep coefficient and $\beta(t, t_0)$ is a coefficient representing the development of creep with time after loading. The notional creep coefficient is defined by:

$$\phi_{c0} = \phi_{RH} \cdot \beta(f_{cm}) \cdot \beta(t_0) \tag{2}$$

where ϕ_{RH} is a factor depending of the relative humidity, $\beta(f_{cm})$ is a factor depending on the strength of the concrete () and $\beta(t_0)$ is a factor depending of the effect of concrete age at the time of the applied load. These factors are defined, in our case with $f_{cm} > 35$ MPa, by respectively:

$$\phi_{RH} = \left[1 + \frac{1 - (RH/100)\%}{0.1(h_0)^{1/3}} \cdot \alpha_1\right] \cdot \alpha_2 \tag{3}$$

$$\beta(f_{cm}) = \frac{16.8}{\sqrt{f_{cm}}} \tag{4}$$

$$\beta(t_0) = \frac{1}{(0.1 + t_0^{0.20})} \tag{5}$$

f_{cm} being the mean compressive cylinder strength (in MPa) and defined by $f_{cm} = f_{ck} + 8$ MPa

The time evolution of the creep is taken into account with:

$$\beta(t, t_0) = \left(\frac{t - t_0}{\beta_H + t - t_0}\right)^{0.3} \tag{6}$$

where β_H is defined, for $f_{cm} \geq 35$ MPa, by

$$\beta_H = 1.5[1 + (0.012\,RH)^{18}]h_0 + 250\alpha_3 > 1500\alpha_3 \tag{7}$$

and t_0 can be corrected to take into account the influence of high temperature and the type of cement (α) with

$$t_0 = t_{0,T}\left[\frac{9}{1 + {t_{0,T}}^{1.2}} + 1\right]^{\alpha} \tag{8}$$

where $t_{0,T}$ is the temperature-adjusted age of concrete at loading in days.

The correction factors α_1, α_2, α_3, in equations (3) and (6) taking into account the influence of the concrete strength are defined following the expressions:

$$\alpha_1 = \left[\frac{35}{f_{cm}}\right]^{0.7}; \alpha_2 = \left[\frac{35}{f_{cm}}\right]^{0.2}; \alpha_3 = \left[\frac{35}{f_{cm}}\right]^{0.5} \tag{9}$$

For the shrinkage strains, this model assumes a decomposition between the autogenous (ε_{ca}) and the drying (ε_{cd}) shrinkage strains as:

$$\varepsilon_{cs}(t) = \varepsilon_{cd}(t) + \varepsilon_{ca}(t) \tag{10}$$

The equations are summarized below for both contributions of the drying and of the autogenous shrinkage:

Drying shrinkage

$$\varepsilon_{cd}(t) = \beta_{ds}(t, t_s).k_h.\varepsilon_{cd0} \tag{11}$$

$$\beta_{ds}(t, t_s) = \frac{(t - t_s)}{(t - t_s) + 0.04\sqrt{{h_0}^3}} \tag{12}$$

$$\varepsilon_{cd0} = 0.85\left[(220 + 110\alpha_{ds1}) \cdot \exp\left(-\alpha_{ds2}\frac{f_{cm}}{10}\right)\right] \cdot 10^{-6} \cdot \beta_{RH} \tag{13}$$

$$\beta_{RH} = 1.55\left[1 - \left(\frac{RH}{100}\right)^3\right] \tag{14}$$

Autogenous shrinkage

$$\varepsilon_{ca}(t) = \beta_{as}(t) \cdot \varepsilon_{ca}(\infty) \tag{15}$$

$$\beta_{as}(t) = 1 - \exp\left(-0.2\sqrt{t}\right) \tag{16}$$

$$\varepsilon_{ca}(\infty) = 2.5(f_{ck} - 10) \times 10^{-6} \tag{17}$$

where α_{ds1} and α_{ds2} are factors depending on the type of cement which are respectively 4 and 0.12 for the class N cement used for the Connecting Gallery; h_0 is the notional size of the cross-section of the member defined by $h_0 = 2Ac/u$ where A_c is the cross sectional area of the concrete (mm^2) and u is the perimeter in contact with the atmosphere (in mm).

The model parameters for both creep and shrinkage were fitted with laboratory creep tests performed by UGent (De Pauw and De Schutter 2003) on concrete samples taken from spare segments. Figure 20 presents the comparison between the Eurocode2 model and the experimental results (creep and shrinkage strain as function of time) obtained with two concrete samples loaded at a constant value of 36.7 MPa during one year. A relatively good agreement is obtained between the model and the experimental results.

To calculate the stress in the Connecting Gallery segments, a constant temperature of 22°C and a

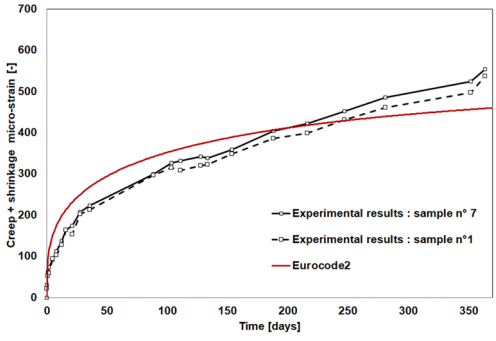

Fig. 20. Comparison between the Eurocode2 model (EN 1992-1-1 2004) and the experimental results (creep and shrinkage strain) obtained at UGent (De Pauw and De Schutter 2003) for two concrete samples loaded at a constant value of 36.7 MPa during one year.

constant relative humidity of 50% were imposed to represent the environmental conditions in the HADES URL. The segments are made from C75/90 concrete and all mechanical properties are derived from the Eurocode2 model. The notional size (h_0) is 800 mm for the Connecting Gallery segments and the age of the concrete at the time of loading depends on each segment.

The stresses at the location of the strain gauges can be calculated for the same segments in ring 30 used to describe the strain evolution above. These segments illustrate the general behaviour observed in all of the instrumented rings. The proximity of the ring 30 to the PRACLAY Gallery allows to see the changes in the strain evolution induced by the large-scale PRACLAY Heater Test.

Figure 21 shows the evolution of the stresses where a quick increase at the beginning of the monitoring is observed. This is due to the rapid augmentation of the clay pressure against the lining. After this augmentation, the rate slows down and the stresses at the invert decrease. The start of the PRACLAY Heater Test perpendicular to the Connecting Gallery can be seen with a temporary change in the evolution rate at the end of 2014. The value of the stresses in these segments is below 30 MPa at the location of the strain gauges, which is much lower than the ultimate strength of the C75/90 concrete. This demonstrates that, at least during the monitoring period, the safety margins against segment rupture are sufficient. Any such rupture could lead to a lack of stability and safety concerns.

The stress analysis was performed for three instrumented rings. Figure 22 presents a comparison of the stresses near the intrados and near the extrados between these three rings at the end of 2002, 2012 and 2020. The stress evolution is very similar for the three rings. In 2002, the stress distribution along the azimuth was rather uniform. At the end of 2012 and 2020, the distribution changed in shape and there was a difference between the springline and the crown and invert (top and bottom) compared with 2002. This change in distribution is the result of the ovalization of the gallery with time (see Fig. 16). Despite this ovalization, the stresses in all of the strain gauges remain in compression and do not exceed the allowable stress.

Nevertheless, as the stresses at the surface of the segments are larger/lower than inside the segments and the stresses continue to evolve, monitoring of the Connecting Gallery will continue to be important to ensure the safe operation of the HADES URL. In addition, the further monitoring will strengthen our understanding of the long-term behaviour of galleries built in poorly indurated clays.

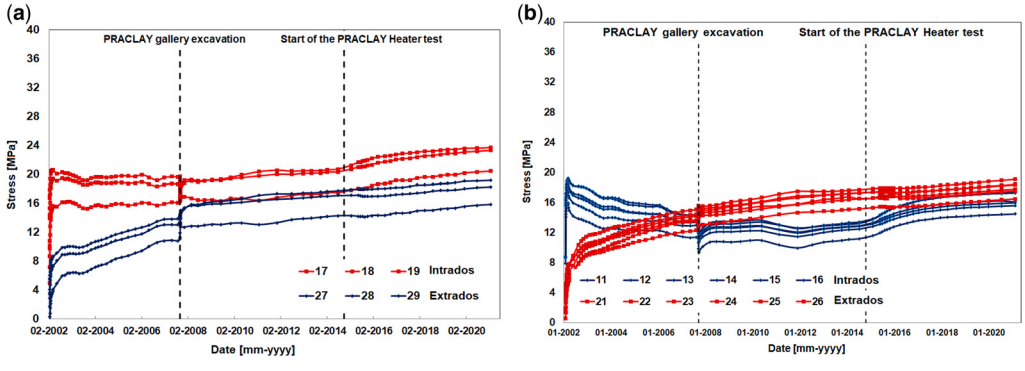

Fig. 21. Evolution of the stresses in two segments of ring 30 taking into account the creep law proposed in Eurocode2 (EN 1992-1-1 2004): (**a**) segment S2 and (**b**) segment S6.

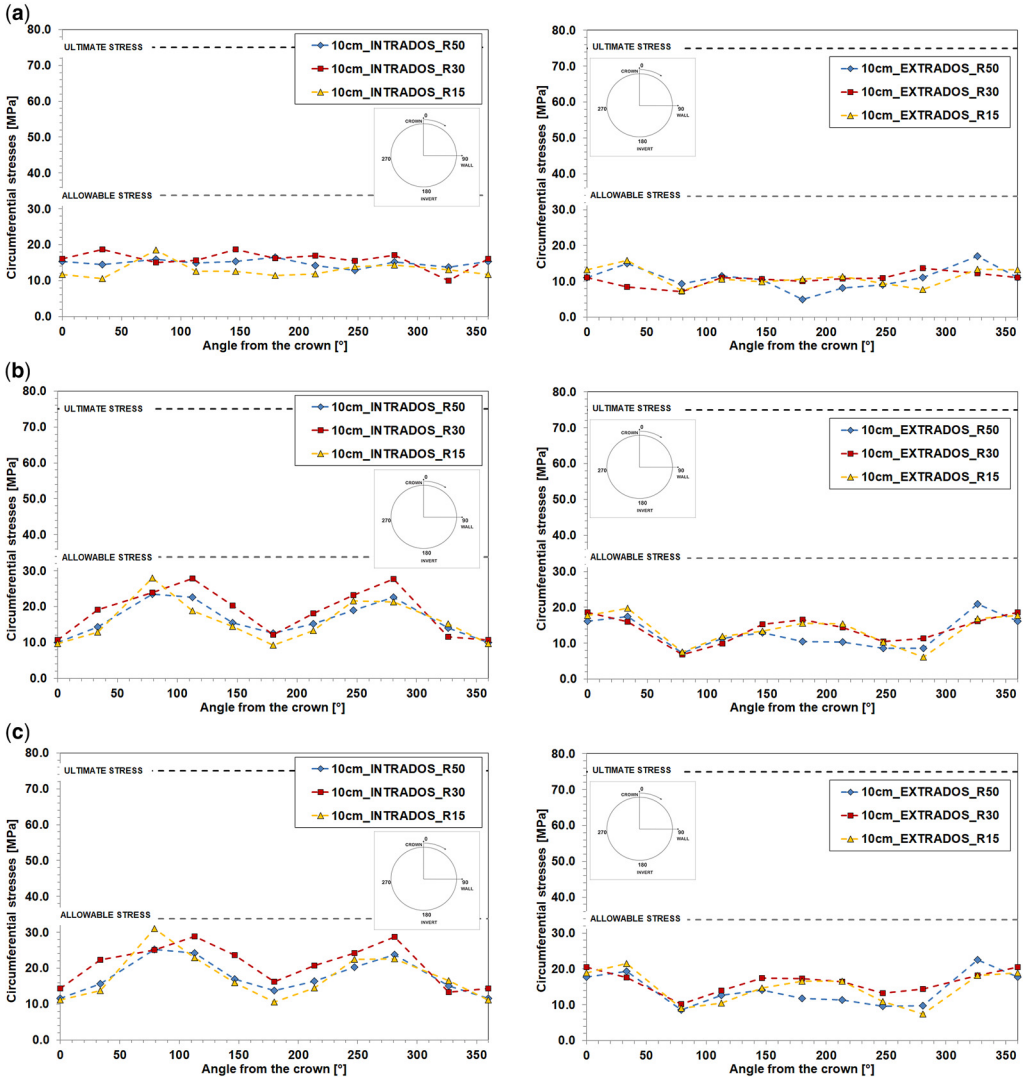

Fig. 22. Stress distribution along the circumference for the three instrumented rings at the intrados and the extrados at the end of (**a**) 2002, (**b**) 2012 and (**c**) 2020.

Monitoring results in GRD4 gallery of the Meuse/Haute-Marne URL

Since 2005, the construction of a network of galleries at the Meuse/Haute-Marne URL (Armand *et al.* 2015) has allowed understanding of the near-field response of the Callovo-Oxfordian claystone to the excavation of the galleries. Observations and measurements were carried out for different excavation methods and types of gallery support. These highlight the importance of the orientation of the galleries with respect to the *in situ* stress field. This stress field is anisotropic with major and minor horizontal principal stresses (Fig. 23). The vertical stress is nearly equal to the minor stress and the weight of the earth. The major horizontal principal stress is oriented N155E (Wileveau *et al.* 2007). The following lessons can be drawn (Armand *et al.* 2014, 2015):

- The fractures are similar for all the excavated structures (diameter, orientation, digging method) with a predominance of shear fracturing.
- The orientation of the galleries in relation to the main horizontal stress plays a role in the fracture pattern induced around the structures: the extension of the fractures is mainly horizontal for the

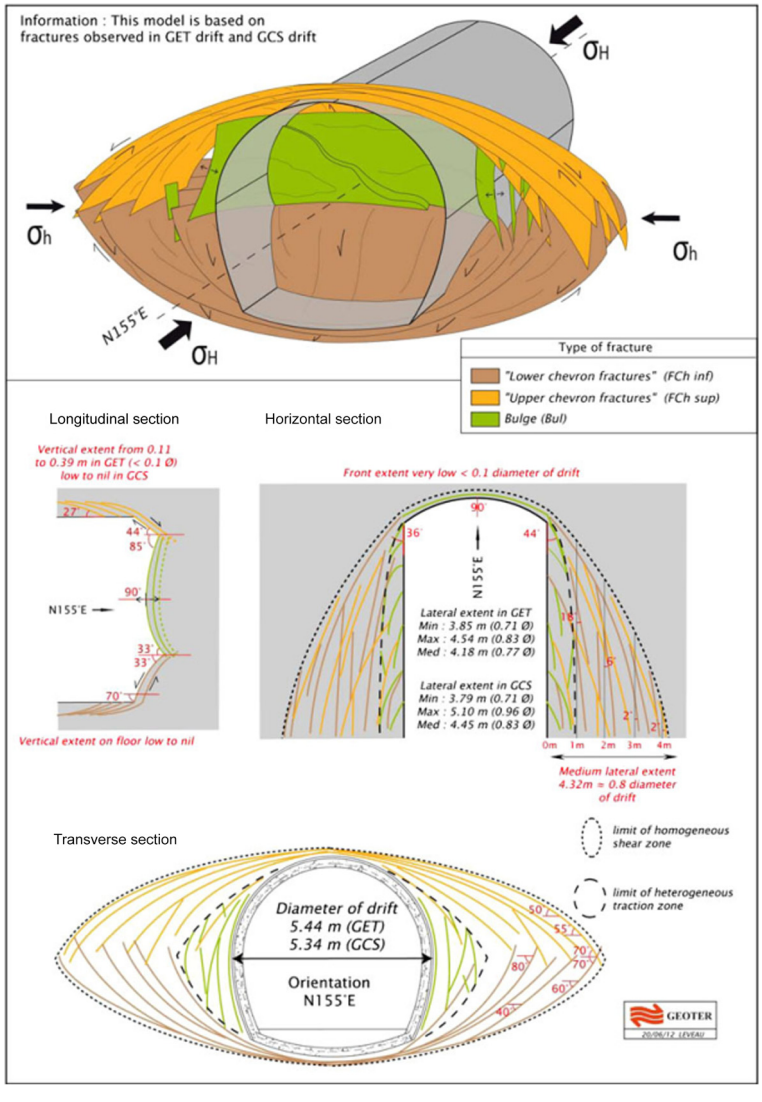

Fig. 23. Conceptual model for induced fractures network (shear and extensional fractures) for the gallery parallel to the major horizontal stress from Armand *et al.* (2014).

ones parallel to the main horizontal stress (despite a quasi-isotropic stress state in the section) while it is mainly vertical for galleries parallel to the minor horizontal stress.

- The damaged zone systematically comprises two zones: one with a connected fractured zone of extensional and shear fractures, and one with 'discrete' fracturing with only shear fractures.
- The geometry and time of emplacement of the lining play a role in the extension and density of induced fracturing. The 'late' installation of the lining (e.g. for a TBM with point attack for which the clamping can only be carried out at the earliest at the exit of the TBM skirt) leads to a greater extension of the fractured zone, which however remains limited.
- There is no scale effect between galleries with a diameter of 5 m and those with a diameter of 9 m.

Figure 23 (Armand *et al.* 2014) illustrates the excavation induced fractures observed around galleries parallel to the major horizontal stress. The general shape with shear chevron-like fractures is similar to that observed in the HADES URL (Figs 18 & 19). At the Meuse/Haute-Marne URL the chevron fractures are also accompanied by extensional factures

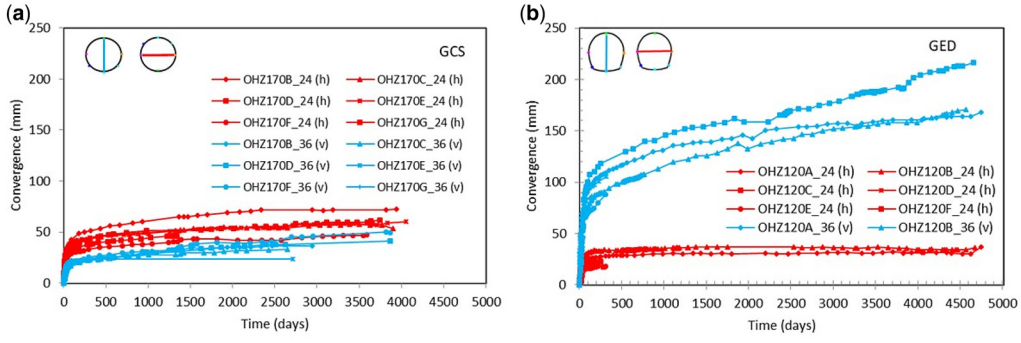

Fig. 24. Convergence measurement of the GCS and GED galleries (**a**) parallel and (**b**) perpendicular, respectively, to the major horizontal stress.

which are related to a higher stress level compared with the strength of the claystone.

Armand *et al.* (2013, 2017) shows that the convergence of the galleries is asymmetric regardless of their orientation or the type of support (galleries with support close to the working face by sliding arches and/or shotcrete with compressible wedge, unsupported micro-tunnel demonstrators). The larger convergence is in the direction of the greatest extension of the fractured zone. Examples of convergence measurements are given in Figure 24 for the gallery GCS (parallel to the major horizontal stress) and GED (perpendicular to the major horizontal stress). The figure shows a rapid evolution of the convergence in the first months of excavation (between 3 and 6 months) followed by an 'asymptotic' evolution of the convergence in the longer term. This anisotropic character of the convergence can be taken into account by assuming that the gallery section will deform into an elliptical shape (Guayacán-Carrillo *et al.* 2016).

Over the monitoring period of around 10 years, the deformation rates continue to decrease over time and reach velocities lower that 10^{-11} s^{-1}. The ratio of vertical to horizontal convergence (C_v/C_h) is about 0.5 and 4–5 for galleries parallel and perpendicular to the major horizontal stress, respectively.

With this anisotropic character of the convergence, an anisotropic loading of the lining can be expected when installing a rigid lining, as is the case for the Connecting Gallery in HADES URL. This is what Andra wanted to study in the Meuse/Haute-Marne URL. The other question is whether the use of a compressible grouting mortar can reduce the loading (i.e. decrease stresses) on the lining and 'dampen' the effect of the convergence.

One of the difficulties when analysing the concrete ring deformation is evaluating the different phenomena that have an impact on the measurement, such as shrinkage, creep, temperature and humidity. Shrinkage (autogenous and drying) was evaluated in different ways and on different sample sizes (with or without reinforcements). In order to determine the intrinsic deformation of the concrete, data from a reference segment (segment not mechanically loaded) are used to apply a correction. That correction takes into account a large part of the shrinkage and climatic deformation.

The measured deformation for the two grouted zones without correction of the gallery temperature is shown in Figure 25. The deformation increase is faster when a classical mortar (A22) is used. It is also noticed that the strains continue to increase in the same way as for the Connecting Gallery in the HADES URL. Figure 26 presents the corrected deformations along the circumference for rings A42 and A62 at different times. It shows an anisotropic loading effect with opposite deformations and stresses at the intrados and the extrados. This anisotropic mechanical effect is consistent with the expected convergence anisotropy showing a convergence that is greater in the horizontal direction for galleries oriented along the major horizontal stress (Fig. 24). This anisotropic loading is observed early after the excavation of the gallery. Figure 25 also shows that the deformations in the ring with compressible grouting mortar are smaller than in rings that are grouted using the classical mortar. It shows that the elastoplastic behaviour of the grouting plays a dampening role and reduce the loading of the lining.

All those observations indicate that, although Boom Clay and Callovo-Oxfordian claystone have different properties (the Boom Clay is a poorly indurated clay while the Callovo-Oxfordian clay is a stiff claystone), there are similarities when comparing the clay/claystone–structure interaction between tunnels in both geological formations. A finding that applies to both formations is that the loading of the galleries kept increasing over the monitoring period.

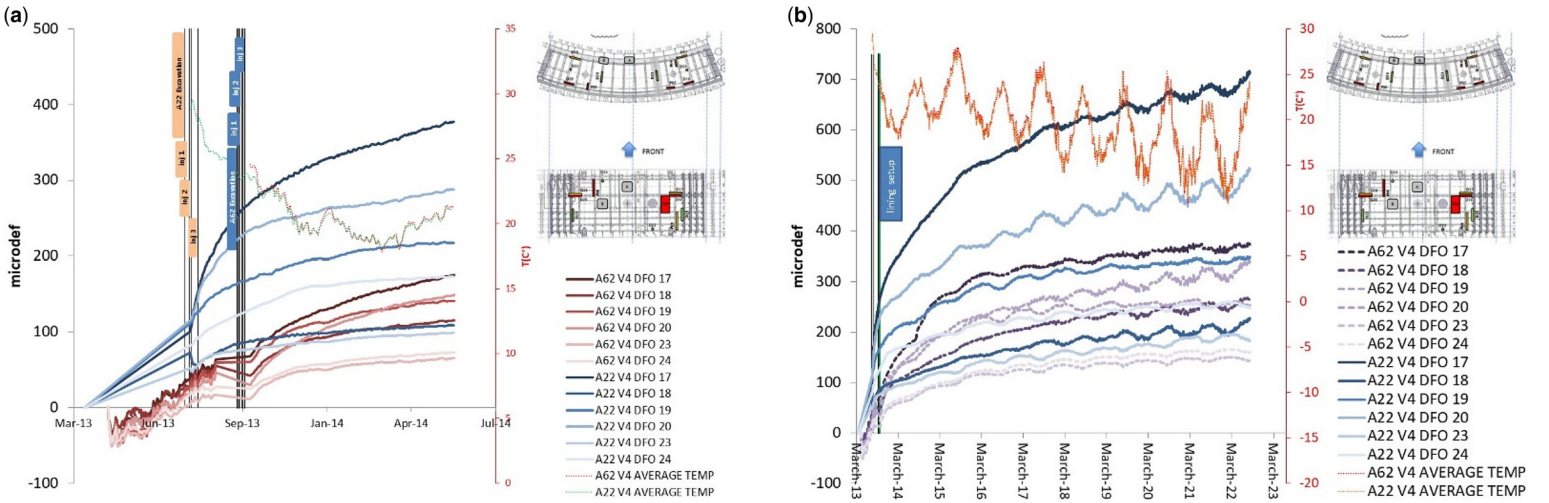

Fig. 25. Comparison of raw deformation (negative strain in compression) in the V4 segment lining for the two backfill grout zones: A22 (classical grout) and A62 (compressible grout zone): (**a**) short term during and after emplacement and (**b**) over 8 years.

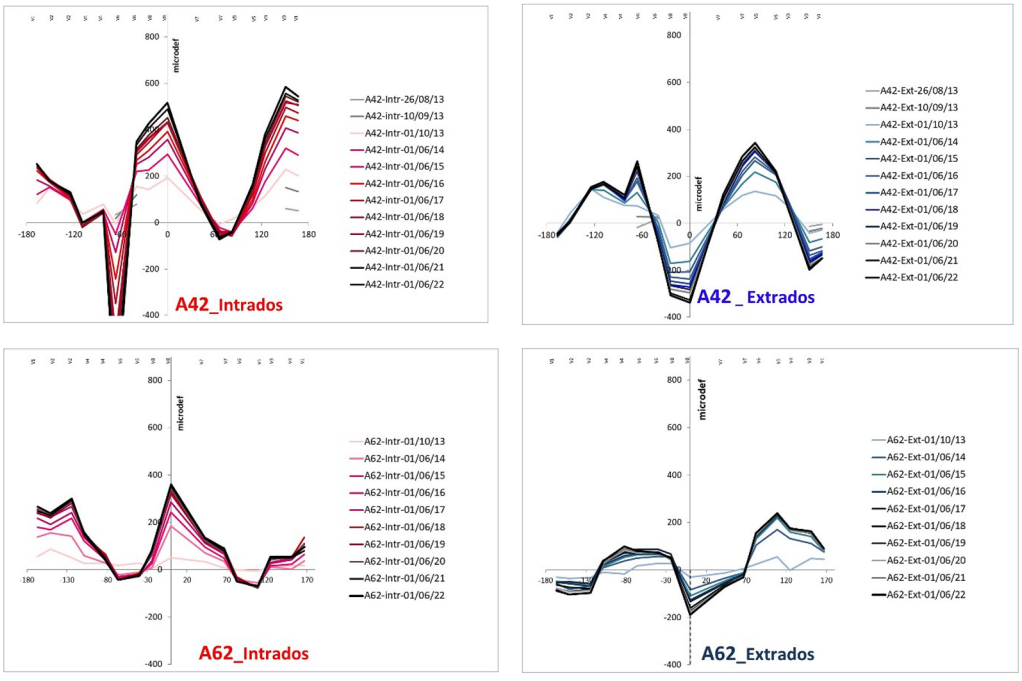

Fig. 26. Evolution of the corrected circumferential strains (μ strain) on the extrados and the intrados of the A42 (classical grout zone) and A62 (compressible grout zone) rings.

Conclusions

The continuous monitoring of the vibrating wire strain gauges in the Connecting Gallery in the HADES URL shows that the strains have been steadily increasing since the excavation of the gallery. The evolution of these strains is different depending on the angular position in the ring. This is caused by the anisotropic *in situ* stress conditions and results in the deformation of the lining into a horizontal egg shape.

The calculated stresses at the level of the sensors show that the stresses steadily increase and that the magnitude of the stresses remains below the ultimate strength of the concrete. No abnormal or sudden changes in the measured strains occurred. This smooth evolution confirms the stability of the gallery. However, as the stresses continue to increase, monitoring of the Connecting Gallery will continue to be important to ensure the safe operation of the HADES URL.

A comparison between the behaviour of the Connecting Gallery in HADES URL and the behaviour of the GRD4 gallery of the Meuse/Haute-Marne URL indicates that, although the Boom Clay and Callovo-Oxfordian claystone are different, there are similarities in the interaction behaviour between the clay/claystone and the tunnels. This study has demonstrated that, for these two geological formations, their mechanical anisotropy and the anisotropic *in situ* stress states have the same major impact on the deformation modes of the galleries. The gallery deformation increases with time owing to the visco-plastic behaviour of the clay/claystone, which causes the load on the lining to increase over the duration of the observations. This load continues to increase even after decades. This highlights the importance of taking these anisotropies and this long-term behaviour into account when designing a future deep geological repository.

Acknowledgements We are grateful to ENGIE TRACTEBEL for their collaboration and their help in the analysis of the Connecting Gallery state of stress.

Competing interests The authors declare that they have no known competing financial interests or personal relationships that could have appeared to influence the work reported in this paper, except from the agencies to which the authors are affiliated.

Author contributions **AD**: investigation (lead), methodology (lead), writing – original draft (lead), writing – review & editing (equal); **MS**: investigation (supporting), methodology (supporting), writing – review & editing

(supporting); **GA**: investigation (supporting), writing – review & editing (supporting); **JZ**: investigation (supporting); **TG**: investigation (supporting), writing – review & editing (supporting); **GC**: writing – review & editing (supporting); **JV**: writing – review & editing (supporting); **XL**: investigation (supporting), methodology (supporting), writing – review & editing (supporting); **DL**: project administration (supporting), writing – review & editing (supporting); **SL**: investigation (supporting), writing – original draft (supporting), writing – review & editing (supporting).

Funding This research received no specific grant from any funding agency in the public, commercial or not-for-profit sectors.

Data availability The data that support the findings of this study are available from EIG EURIDICE, SCK CEN and NIRAS/ONDRAF but restrictions apply to the availability of these data, which were used under licence for the current study, and so are not publicly available. Data are, however, available from the authors upon reasonable request and with permission of EIG EURIDICE, SCK CEN and NIRAS/ONDRAF.

References

Armand, G., Noiret, A., Zghondi, J. and Seyedi, D.M. 2013. Short- and long-term behaviors of drifts in the Callovo-Oxfordian claystone at the Meuse/Haute-Marne Underground Research Laboratory. *Journal of Rock Mechanics and Geotechnical Engineering*, **5**, 221–230, https://doi.org/10.1016/j.jrmge.2013.05.005

Armand, G., Leveau, F. *et al*. 2014. Geometry and properties of the excavation-induced fractures at the Meuse/Haute-Marne URL drifts. *Rock Mechanic and Rock Engineering*, **47**, 21–41.

Armand, G., Plas, F. and Bosgiraud, J.-B. 2015. L'apport du Laboratoire souterrain de l'Andra pour le choix et la mise au point des techniques de creusement des ouvrages souterrains du projet de stockage de déchets radioactifs Cigéo, *Tunnel et Ouvrages Souterrain (AFTES)*, **250**, 251–268.

Armand, G., Bumbieler, F., Conil, N., de La Vaissière, R., Bosgiraud, J.-M. and Vu, M.N. 2017. Main outcomes from in situ thermo-hydro-mechanical experiments programme to demonstrate feasibility of radioactive high-level waste disposal in the Callovo-Oxfordian claystone. *Journal of Rock Mechanics and Geotechnical Engineering*, **9**, 415–427, https://doi.org/10.1016/j.jrmge.2017.03.004

Bastiaens, W., Bernier, F., Buyens, M., Demarche, M., Li, X.L., Linotte, J.M. and Verstricht, J. 2003. *The Connecting Gallery – the extension of the HADES underground research facility at Mol, Belgium*. EURIDICE report 03-294. ESV EURIDICE, Mol.

Bastiaens, W., Bernier, F. and Verstricht, J. 2006. 25 years of underground engineering in a plastic clay formation: the HADES underground research facility. *Proceedings of the 5th International Conference of TC28 of the ISSMGE on Geotechnical Aspects of Underground Construction in Soft Ground*, London, 795–801.

Bernier, F., Li, X.L., Verstricht, J. and Barnichon, J.D. 2003. *CLIPEX: Clay Instrumentation Programme for the extension of an underground research laboratory*. EC contract FI4W-CT96-0028, Final report, Commission of the European Communities. Nuclear Science and Technology EUR 20619.

Bernier, F., Li, X.L. and Bastiaens, W. 2007. Twenty-five years' geotechnical observation and testing in the Tertiary Boom clay formation. *Géotechnique*, **57**, 229–237, https://doi.org/10.1680/geot.2007.57.2.229

Carraretto, S., Noiret, A. and Zghondi, J. 2015. TBM at the Meuse/Haute-Marne Underground Research Laboratory. *ITA WTC 2015 Congress and 41st General Assembly*, 22–28 May, Dubrovnik.

Chen, G., Li, X., Dizier, A., Verstricht, J., Sillen, X. and Levasseur, S. 2023. Characterization of Boom Clay anisotropic THM behaviour based on two heating tests at different scales in the HADES URL. *Geological Society, London, Special Publications*, **536**, https://doi.org/10.1144/SP536-2022-72

De Beer, A., Carpentier, R., Manfroy, P. and Heremans, R. 1977. Preliminary studies of an underground facility for nuclear waste burial in a tertiary clay formation. *Rockstore Conference*, Stockholm, **3**, 771–780.

Delay, J., Vinsot, A., Krieguer, J.-M., Rebours, H. and Armand, G. 2007. Making of the underground scientific experimental programme at the Meuse/Haute-Marne underground research laboratory, North Eastern France. *Physics and Chemistry of the Earth, Parts A/B/C*, **32**, 2–18, https://doi.org/10.1016/j.pce.2006.04.033

De Pauw, P. and De Schutter, G. 2003. Laboratorium Magnel voor Betononderzoek, Universiteit van Gent, Proeven op Betonkernen, Proefverslag 2002/514-B – PDP/MS, 16.

Dizier, A., Chen, G.J., Li, X.L., Leysen, J., Verstricht, J., Troullinos, I. and Rypens, J. 2016. *The Start-up Phase of the PRACLAY Heater Test*. EUR_PH_16_025, Mol, Belgium.

Dizier, A., Chen, G.J., Verstricht, J., Li, X.L., Sillen, X. and Levasseur, S. 2021. The large-scale in situ PRACLAY heater test: first observations on the in situ thermo-hydro-mechanical behaviour of Boom Clay. *International Journal of Rock Mechanics and Mining Sciences*, **137**, 104558, https://doi.org/10.1016/j.ijrmms.2020.104558

EN 1992-1-1. 2004. Eurocode2: Design of Concrete Structures – Part 1.1: General Rules and Rules for Buildings.

François, B., Labiouse, V., Dizier, A., Marinelli, F., Charlier, R. and Collin, F. 2014. Hollow cylinder tests on boom clay: modelling of strain localization in the anisotropic excavation damaged zone. *Rock Mechanics and Rock Engineering*, **47**, 71–86, https://doi.org/10.1007/s00603-012-0348-5

Funcken, R., Gonze, P., Vranken, P., Manfroy, P. and Neerdael, B. 1983. *Construction of an experimental laboratory in a deep clay formation*. Eurotunnel Conference 1983, Basel, Switzerland, 79–85.

Guayacán-Carrillo, L.M., Sulem, J., Seyedi, D.M., Ghabezloo, S., Noiret, A. and Armand, G. 2016. Analysis of long-term anisotropic convergence in drifts excavated in Callovo-Oxfordian claystone. *Rock Mechanics and*

Rock Engineering, **49**, 97–114, https://doi.org/10.1007/s00603-015-0737-7

Labiouse, V., Sauthier, C. and You, S. 2014. Hollow cylinder experiments of galleries in Boom Clay Formation. *Rock Mechanics and Rock Engineering*, **47**, 43–55, https://doi.org/10.1007/s00603-012-0332-0

Li, X.L., Neerdael, B., Raymaekers, D. and Sillen, X. 2023. The construction of the HADES underground research laboratory and its role in the development of the Belgian concept of a deep geological repository. *Geological Society, London, Special Publications*, **536**, https://doi.org/10.1144/SP536-2022-101

Mertens, J., Bastieans, W. and Dehandschutter, B. 2004. Characterisation of induced discontinuities in the Boom Clay around the underground excavations (URF, Mol, Belgium). *Applied Clay Science*, **26**, 413–428, https://doi.org/10.1016/j.clay.2003.12.017

Neerdael, B., De Bruyn, D., Mair, R.J. and Taylor, R.N. 1992. The Hades project at Mol: geomechanical behaviour of Boom Clay. *In*: *Workshop on Pilot Tests on Radioactive Waste Disposal in Underground Facilities*, Braunschweig, June 1991. European Commission, EUR 13985, 223–238.

ONDRAF/NIRAS 2013. *Research, Development and Demonstration (RD&D) plan for the geological disposal of high level and/or long-lived radioactive waste including irradiated fuel if considered as waste*. State-of-the-art report as of December 2012. Belgian Agency for Radioactive Waste for Enriched Fissile Materials. NIROND-TR 2013-12 E.

Rousset, G. 1988. *Comportement mécanique des argiles profondes, application au stockage de déchets radioactifs*. PhD thesis, École Nationale des Ponts et Chaussées.

Rousset, G. 1990. Les sollicitations à long terme des revêtements des tunnels. *Revue Française de Géotechnique*, **53**, 5–20, https://doi.org/10.1051/geotech/1990053005

Salehnia, F. 2015. *From some obscurity to clarity in Boom Clay behavior: analysis of its coupled hydro-mechanical response in the presence of strain localization*. PhD thesis, Université de Liège.

Van Marcke, P., Li, X.L., Bastiaens, W., Verstricht, J., Chen, G.J., Leysen, J. and Rypens, J. 2013. *The design and installation of the PRACLAY In-Situ Experiment*. EURIDICE report 13-129.

Verstricht, J., Li, X.L., Leonard, D. and Van Geet, M. 2022. Assessment of sensor performance in the context of geological radwaste disposal – a first case study in the Belgian URL HADES. *Geomechanics for Energy and the Environment*, https://doi.org/10.1016/j.gete.2021.100296

Villar, M.V., Armand, G. *et al.* 2020. D7.1 HITEC. *Initial state-of-the-art on THM behaviour of (i) buffer clay materials and of (ii) host clay materials*. Deliverable D7.1 HITEC. EURAD Project, Horizon 2020 No. 847593, https://www.ejp-eurad.eu/sites/default/files/2021-04/EURAD%20-%20D7.1%20Initial%20SotA%20HITEC.pdf

Wileveau, Y., Cornet, F.H., Desroches, J. and Blümling, P. 2007. Complete in situ stress determination in an argillite sedimentary formation. *Physics and Chemistry of the Earth*, **32**, 866–878, https://doi.org/10.1016/j.pce.2006.03.018

Zghondi, J., Carraretto, S., Noiret, A. and Armand, G. 2015. Monitoring and behavior of an instrumented concrete lining segment of a TBM excavation experiment at the Meuse Haute-Marne Underground Research Laboratory. *Proceedings of the 10th International Conference on Mechanics and Physics of Creep, Shrinkage, and Durability of Concrete and Concrete Structures*, 21–23 September, Vienna, Austria.